International Journal of Mass Spectrometry 299 (2011) 102–112

Contents lists available at ScienceDirect

International Journal of Mass Spectrometry

journal homepage: www.elsevier.com/locate/ijms

Damping effects in Penning trap mass spectrometry

S. George[a,b,*], K. Blaum[b,c], M. Block[d], M. Breitenfeldt[e,1], M. Dworschak[a,d], F. Herfurth[d], A. Herlert[f], M. Kowalska[b,f], M. Kretzschmar[a], E. Minaya Ramirez[d], D. Neidherr[a], S. Schwarz[g], L. Schweikhard[e]

[a] Institut für Physik, Johannes Gutenberg-Universität, 55099 Mainz, Germany
[b] Max-Planck-Institut für Kernphysik, 69117 Heidelberg, Germany
[c] Physikalisches Institut, Ruprecht-Karls-Universität, 69120 Heidelberg, Germany
[d] GSI Helmholtzzentrum für Schwerionenforschung Darmstadt, Planckstraße 1, 64291 Darmstadt, Germany
[e] Institut für Physik, Ernst-Moritz-Arndt-Universität, 17487 Greifswald, Germany
[f] CERN, Physics Department, 1211 Geneva 23, Switzerland
[g] NSCL, Michigan State University, East Lansing, MI 48824-1321, USA

ARTICLE INFO

Article history:
Received 20 April 2010
Received in revised form
29 September 2010
Accepted 29 September 2010
Available online 8 October 2010

Keywords:
Penning trap
Ion motion
Mass spectrometry

ABSTRACT

Collisions of ions with residual gas atoms in a Penning trap can have a strong influence on the trajectories of the ions, depending on the atom species and the gas pressure. We report on investigations of damping effects in time-of-flight ion-cyclotron resonance mass spectrometry with the Penning trap mass spectrometers ISOLTRAP at ISOLDE/CERN (Geneva, Switzerland) and SHIPTRAP at GSI (Darmstadt, Germany). The work focuses on the interconversion of the magnetron and cyclotron motional modes, in particular the modification of the resonance profiles for quadrupolar excitation due to the damping effect of the residual gas. Extensive experiments have been performed with standard and Ramsey excitation schemes. The results are in good agreement with predictions obtained by analytical continuation of the formulae for the undamped case.

1. Introduction

Penning traps have set milestones in high-precision mass spectrometry of stable and short-lived nuclei [1–3], including most recent investigations beyond the proton drip line [4] and of transfermium nuclides [5] as well as the discovery of a new radon isotope [6]. The mass of a charged particle is linked to the cyclotron frequency in a homogeneous magnetic field, $\nu_c = qB/(2\pi m)$. In a Penning trap [7] charged particles are confined by static electric and magnetic fields. The ion movement consists of three harmonic eigenmotions: the axial oscillation, the magnetron drift, and the cyclotron motion with a modified frequency. In an ideal Penning trap the movement occurs in perfect vacuum, but in reality residual gas is always present. This causes undesirable complications, since the oscillatory motions of the ions in the trap are damped with accompanying energy loss and frequency shifts of the eigenmotions [8–10]. Sometimes, on the other hand, the damping force is of experimental use, such as for mass-selective buffer-gas cooling [11].

In time-of-flight ion-cyclotron resonance (TOF-ICR) [12] mass spectrometry damping of the radial modes shows up in an unwanted line broadening of the resonance as well as in a reduced resonance depth. Both effects increase the uncertainty of the frequency determination. For precision mass measurements the effect of damping on the line profile of a standard quadrupolar excitation has already been addressed by König et al. [13]. The adaption of Ramsey's method of separated oscillatory fields for excitation of the ion motion in a Penning trap [14–18], which is meanwhile routinely used for precision mass measurements of short-lived radionuclides [19–21] required an extension to more general excitation profiles. In this context a new mathematical approach to damping phenomena using analytical continuation of the cyclotron frequency has been introduced recently [8].

In this article we first present the typical experimental setup of TOF-ICR mass spectrometry. Then the explicit expressions including damping effects are derived for the TOF-ICR resonance line shapes for conventional one-pulse excitation and for symmetric two-pulse excitation by quadrupolar rf-fields. In the experimental section data from the Penning trap mass spectrometers ISOLTRAP [22] and SHIPTRAP [23] are compared with the predicted line profiles including damping effects. In particular, two important phenomena have been addressed. The first one is the periodic inter-

* Corresponding author. Present address: NSCL, Michigan State University, East Lansing, MI 48824-1321, USA. Tel.: +1 517 908 7409.
E-mail address: george@nscl.msu.edu (S. George).
[1] Present address: K.U.Leuven, Instituut voor Kernen Stralingsfysica, Celestijnenlaan 200D, B-3001 Leuven, Belgium.

1387-3806/$ – see front matter © 2010 Elsevier B.V. All rights reserved.
doi:10.1016/j.ijms.2010.09.030

conversion of the magnetron and cyclotron mode due to an external quadrupolar rf-field at exactly the resonance frequency. A continuous excitation results in a Rabi-like oscillation between the two modes with an exponentially decreasing amplitude. In the ideal case, neglecting any damping, the conversion time τ_c depends only on the coupling strength of the external field, which is proportional to the rf-field amplitude. Damping due to residual gas affects the conversion time as well as the amplitude of the Rabi oscillations. Since the time scale of the damping in the cyclotron mode is of the same order as the conversion time, a considerable loss in radial energy is expected to be measurable. The second subject concerns the TOF-ICR resonance line shapes of two different excitation schemes, namely one- or two-pulse excitation.

2. Experimental setup

The experimental data presented in this article have been obtained with the Penning trap mass spectrometers ISOLTRAP at ISOLDE/CERN and SHIPTRAP at the velocity filter SHIP/GSI. The experimental procedure at ISOLTRAP is as follows: A 60 keV continuous ion beam delivered from the stable alkali reference ion source is accumulated in a linear gas-filled radio-frequency quadrupolar (RFQ) ion beam cooler and buncher [24]. After a few milliseconds the accumulated ions are transferred in a bunch to the first Penning trap, a cylindrical 4.7 T preparation trap used for mass-selective buffer-gas cooling to remove isobaric contaminations. The preparation trap is followed by the precision trap within a 5.9 T magnet, where the actual frequency determination takes place by means of the TOF-ICR technique. Ions are detected by a channeltron detector [25], which is placed behind the two traps. Here, helium-gas was used in the RFQ as well as in the preparation trap and $^{39}K^+$ ions have been selected to perform the experiments. In order to suppress the gas flow from the preparation to the precision trap a vacuum pump is installed at the transfer section.

The SHIPTRAP facility is, similarly to ISOLTRAP, a double-Penning trap mass spectrometer. For the measurements performed at SHIPTRAP the ion species $^{133}Cs^+$ from a stable alkali reference ion source is injected into the first cylindrical Penning trap with a magnetic field strength of 7 T. It is used for isobaric cleaning and further cooling of the ion motion. The second cylindrical trap, placed in the same magnet, but separated by a 5 cm long pumping barrier for differential pumping [26], is used for the TOF measurement. Because only differential pumping is used to decrease the pressure on the way from the first to the second trap, the gas flow of the buffer-gas in the first trap can be effectively used to adjust the residual gas pressure in the precision trap for the experiments described in this paper. Behind the precision trap a micro-channel-plate (MCP) detector is placed for particle detection. Some frequencies, which are important in the context of damping effects, are listed in Table 1.

Both experiments use the well-established TOF-ICR detection method to determine the cyclotron frequency ν_c. To this end, the ion ensemble is captured in the center of the precision Penning trap in order to avoid initially large amplitudes of the radial and axial modes. All ions are excited by an azimuthal, dipolar rf-field at their magnetron frequency, such that they have a defined magnetron radius $R_-(0)$ [27]. Subsequently, a quadrupolar driving field is applied at the cyclotron frequency. In the absence of damping a suitably chosen amplitude A_q and duration τ_{conv} leads to a full conversion from the magnetron into the cyclotron mode assuming the frequency of the quadrupolar driving field is $\nu_q = \nu_c$ [28,29]. The final cyclotron radius is then as large as the magnetron radius prior to the quadrupolar excitation $R_+(\tau_{conv}) = R_-(0)$. Due to the much higher frequency of the cyclotron mode as compared to the magnetron mode, the conversion is accompanied by an increase of the radial kinetic energy by about six orders of magnitude.

Table 1
Eigenfrequencies of the singly-charged ions for the precision Penning traps of ISOLTRAP (magnetic field strength $B = 5.9$ T, trap voltage $U = 10$ V, characteristic trap dimension $d^2 = 104.5$ mm^2) and of SHIPTRAP ($B = 7.0$ T, $U = 10$ V, $d^2 = 331.2$ mm^2).

Experiment	Ion species	ν_c/MHz	ν_z/kHz	ν_-/Hz
ISOLTRAP	$^{39}K^+$	2.3	72	1078
SHIPTRAP	$^{85}Rb^+$	1.3	88	1350
SHIPTRAP	$^{133}Cs^+$	0.8	47	1350

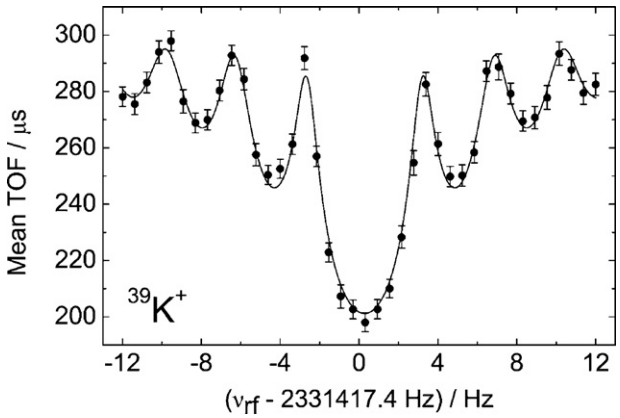

Fig. 1. Time-of-flight ion-cyclotron-resonance data taken at ISOLTRAP for $^{39}K^+$. The excitation time was $\tau = 300$ ms, the damping constant $\gamma = 1$ Hz. The solid line shows a fit of the theoretically expected line shape to the data according to Eq. (36). For further details see text.

This energy can be probed via a time-of-flight measurement. A resonance curve as shown in Fig. 1, obtained by scanning the excitation frequency around the expected cyclotron frequency, is recorded. The cyclotron frequency can be extracted from a fit of the expected resonance line shape to the experimental data [13,15]. For this purpose the fitting routine incorporates the following set of free parameters: The cyclotron frequency ν_c represents the center frequency of the resonance, initial magnetron radius $R_-(0)$ and cyclotron radius $R_+(0)$ determine the radial position and energy before the quadrupolar driving field is applied. The amplitude and duration of the rf-field have to be chosen such that a full conversion from magnetron into cyclotron motion is obtained. If this requirement is not fulfilled the resonance line shape will change [13]. Therefore a parameter called "degree of conversion" is introduced. As discussed below, when damping forces are acting the conversion process must compensate energy losses in the cyclotron mode due to damping and the maximal degree of conversion no longer represents a full conversion of the magnetron mode. The damping force is accounted for by the damping coefficient γ, which is treated here also as a free parameter.

3. Theoretical framework

3.1. Basic considerations

The buffer-gas damping of the ion motion in a Penning trap has been studied by various authors [7,9,10,13,30] who assumed a damping force linear in the ion velocity $\vec{v}$, $\vec{F} = -2m\gamma\vec{v}$. The damping coefficient γ can be deduced from the ion mobility K and depends on the choice of buffer-gas, its pressure and temperature, and the ion-atom collision cross-sections [31],

$$2m\gamma = \frac{q}{K} = \frac{q}{K_0} \cdot \frac{(p/p_0)}{(T/T_0)}, \quad (1)$$

where q is the electric charge of the ions and where the reduced ion mobility K_0 refers to normal atmospheric pressure $p_0 = 10^5$ Pa and room temperature $T_0 = 300$ K. Typical values for K_0 range from 10

to 20 $cm^2/V\,s$ for ions in helium and from 1 to 3 $cm^2/V\,s$ for ions in nitrogen, the higher values being for light ions and the lower values for heavy ions [32,33].

The damping force is included in the Newtonian equations of motion. Their solution provides first of all information about the ion trajectories, while other physical quantities of interest, such as line shapes for the interconversion of magnetron and cyclotron motion, have to be derived from the trajectory functions. For an ideal hyperbolic Penning trap the Newtonian equations of motion read [8]

$$\ddot{x} + 2\gamma\dot{x} - \omega_c\dot{y} - \frac{1}{2}\omega_z^2 x = 0, \tag{2}$$

$$\ddot{y} + 2\gamma\dot{y} + \omega_c\dot{x} - \frac{1}{2}\omega_z^2 y = 0, \tag{3}$$

$$\ddot{z} + 2\gamma\dot{z} + \omega_z^2 z = 0, \tag{4}$$

with the cyclotron frequency $\nu_c = \omega_c/(2\pi)$, and the axial frequency $\nu_z = \omega_z/(2\pi)$. The latter is related to the electrostatic potential difference U between the trap electrodes and the geometric trap parameters r_0, z_0 by $\omega_z = \sqrt{4qU/(m(2z_0^2 + r_0^2))}$ (r_0 = inner radius of the ring electrode, z_0 = shortest distance of the end electrodes from the trap center).

Cylindrical Penning traps, used for example in the SHIPTRAP setup, differ from the ideal hyperbolic Penning trap by additional non-harmonic terms in the electric potential. Theoretical results derived for hyperbolic traps are still applicable in cylindrical traps, provided that (a) the axial ion motion is negligible, and (b) the radius of the azimuthal motion remains small compared to the trap radius r_0. Correction terms can be derived by perturbation methods where necessary.

Recently it was noted [8], using $u = x + iy$, that in the complex combination of the Eqs. (2) and (3) for the azimuthal motion the parameters ω_c and γ occur only in the combination $\bar{\omega}_c = \omega_c - 2i\gamma$,

$$\ddot{u} + i(\omega_c - 2i\gamma)\dot{u} - \frac{1}{2}\omega_z^2 u = 0. \tag{5}$$

Defining the complex variable $\bar{\omega}_c = \omega_c - 2i\gamma$, this opens up the possibility to use analytic continuation in $\bar{\omega}_c$, from the real value $\bar{\omega}_c = \omega_c$ to the complex value $\bar{\omega}_c = \omega_c - 2i\gamma$, to derive results for damped ion motion in the azimuthal modes from corresponding results for undamped ion motion, without having to deal in detail with the trajectory functions. The applicability of the method requires two conditions to be satisfied:

(a) The damping force must be linear in the ion velocity,
(b) there is no coupling between the axial motion and the two azimuthal modes of the ion motion.

The following subsections explain in more detail how the method is applied to derive line shapes for the resonant conversion of pure magnetron motion into cyclotron motion due to quadrupole excitation, using the standard 1-pulse excitation scheme or symmetric 2-pulse Ramsey excitation scheme, starting from the formulas for the undamped motion and obtaining the results for damped motion by analytic continuation.

Considering an ideal hyperbolic Penning trap without damping, let us denote by $\nu_+ = \omega_+/(2\pi)$ the modified cyclotron frequency, and by $\nu_- = \omega_-/(2\pi)$ the magnetron frequency. As is well known we have the relations $\omega_+ = (1/2)(\omega_c + \omega_1)$ and $\omega_- = (1/2)(\omega_c - \omega_1)$ with $\omega_1 = \sqrt{\omega_c^2 - 2\omega_z^2}$. "Analytic continuation in $\bar{\omega}_c$" means that instead of the real quantity ω_c we consider the complex quantity $\bar{\omega}_c = \omega_c - 2i\gamma$ and vary γ from the initial value $\gamma = 0$ (undamped case) to the actual experimental value of the damping constant γ. This implies the replacements

$$\omega_c \to \bar{\omega}_c = \omega_c - 2i\gamma, \tag{6}$$

$$\omega_1 \to \bar{\omega}_1 = \sqrt{\bar{\omega}_c^2 - 2\omega_z^2} = \Re(\bar{\omega}_1) + i\Im(\bar{\omega}_1) = \tilde{\omega}_1 - i\,\tilde{\gamma}_1, \tag{7}$$

$$\omega_\pm \to \bar{\omega}_\pm = \frac{1}{2}(\bar{\omega}_c \pm \bar{\omega}_1) = \Re(\bar{\omega}_\pm) + i\Im(\bar{\omega}_\pm) = \tilde{\omega}_\pm - i\,\tilde{\gamma}_\pm. \tag{8}$$

Here $\Re(\bar{\omega}_i)$ and $\Im(\bar{\omega}_i)$ denote the real and imaginary parts of the complex number $\bar{\omega}_i$. We also use the more convenient notation $\tilde{\omega}_i = \Re(\bar{\omega}_i)$ and $\tilde{\gamma}_i = -\Im(\bar{\omega}_i)$. Straightforward algebra yields the explicit expressions

$$\begin{aligned}\tilde{\omega}_1 &= \Re(\bar{\omega}_1) \\ &= \frac{1}{\sqrt{2}}\sqrt{\sqrt{(\omega_1^2 - 4\gamma^2)^2 + 16\gamma^2\omega_c^2} + (\omega_1^2 - 4\gamma^2)},\end{aligned} \tag{9}$$

$$\begin{aligned}\tilde{\gamma}_1 &= -\Im(\bar{\omega}_1) \\ &= \frac{1}{\sqrt{2}}\sqrt{\sqrt{(\omega_1^2 - 4\gamma^2)^2 + 16\gamma^2\omega_c^2} - (\omega_1^2 - 4\gamma^2)},\end{aligned} \tag{10}$$

in agreement with results derived by conventional methods (see [10], p. 206). To summarize, by the analytic continuation procedure we obtain complex frequencies, whose real parts represent the eigenfrequencies in the proper sense, and whose imaginary parts represent the decay constants of the eigenmodes of the damped Penning trap,

$$\tilde{\omega}_\pm = \frac{1}{2}(\omega_c \pm \tilde{\omega}_1), \tag{11}$$

$$\tilde{\gamma}_\pm = \frac{1}{2}(2\gamma \pm \tilde{\gamma}_1). \tag{12}$$

Note that $\tilde{\gamma}_- \le 0$ so that $\exp[-\tilde{\gamma}_-\tau]$ is increasing with increasing τ.

The solution of the complex equations of motion for the ideal damped Penning trap, Eq. (5), results in

$$\begin{aligned}u(\tau) &= R_+ e^{-i(\tilde{\omega}_+\tau + \chi_+)} + R_- e^{-i(\bar{\omega}_-\tau + \chi_-)} \\ &= \sqrt{(2\hbar/m\omega_1)}\left(\alpha_+(\tau) + \alpha_-^*(\tau)\right).\end{aligned} \tag{13}$$

Here $R_\pm = \sqrt{2\hbar/(m\omega_1)}|\alpha_\pm(0)|$ denotes the initial cyclotron or magnetron radius, respectively, the $\chi_\pm$ are phase parameters, the asterisk means complex conjugation, and the $\alpha_\pm(\tau)$ are the complex oscillator amplitudes, introduced in [15] as the classical analogues of the quantum mechanical annihilation operators for oscillator quanta. They obey the differential equations

$$\dot{\alpha}_+(\tau) = -i\bar{\omega}_+\alpha_+(\tau), \tag{14}$$

$$\dot{\alpha}_-(\tau) = +i\bar{\omega}_-^*\alpha_-(\tau), \tag{15}$$

with the solutions

$$\begin{aligned}\alpha_+(\tau) &= |\alpha_+(0)|e^{-i(\tilde{\omega}_+\tau + \chi_+)} \\ &= |\alpha_+(0)|e^{-\tilde{\gamma}_+\tau}\cdot e^{-i(\tilde{\omega}_+\tau + \chi_+)},\end{aligned} \tag{16}$$

$$\begin{aligned}\alpha_-(\tau) &= |\alpha_-(0)|e^{+i(\bar{\omega}_-^*\tau + \chi_-)} \\ &= |\alpha_-(0)|e^{-\tilde{\gamma}_-\tau}\cdot e^{+i(\tilde{\omega}_-\tau + \chi_-)}.\end{aligned} \tag{17}$$

Here we see that damping factors arise from phase factors with complex frequencies. Therefore throughout this paper a careful treatment of phase factors is of utmost importance.

For $\gamma \ll \omega_c$ the right hand side of Eq. (10) can be expanded as a power series, its first two terms approximate decay constant $\tilde{\gamma}_1$ by

$$\begin{aligned}\tilde{\gamma}_1 &\approx \frac{2\gamma\omega_c}{\sqrt{\omega_1^2 - 4\gamma^2}}\cdot\left(1 - \frac{1}{2}\left(\frac{2\gamma\omega_c}{\omega_1^2 - 4\gamma^2}\right)^2 + \dots\right) \\ &\approx 2\gamma\frac{\omega_c}{\omega_1}\cdot\left(1 - \frac{2\gamma^2\omega_c^2}{\omega_1^4} + \dots\right).\end{aligned} \tag{18}$$

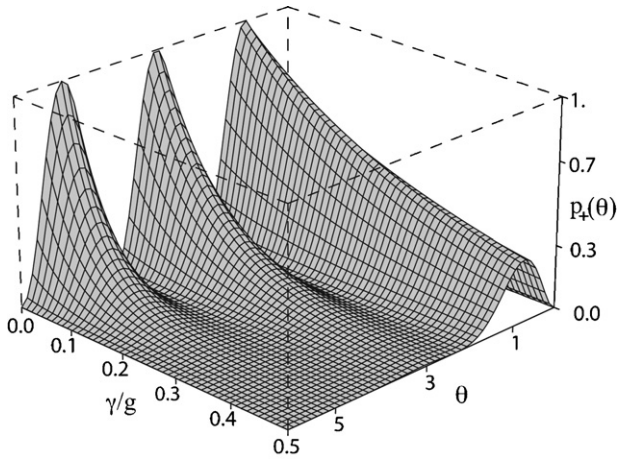

Fig. 2. The excitation function $P_+(\theta, g, \gamma)$ (Eq. (37)), plotted as a function of θ and γ/g, using the approximation $\tilde{\gamma}_1 \approx 2\gamma(\omega_c/\omega_1)$ (Eq. (19)). For $\gamma/g = 0$ the function $P_+(\theta, g, 0)$ represents a Rabi oscillation, for small γ/g we see damped Rabi oscillations, for larger γ/g only the first conversion peak survives the damping effects.

For the frequencies listed in Table 1 we obtain the ratios $\omega_c/\omega_1 = 1.00098$, 1.0046, and 1.0035, respectively. Assuming moreover $\gamma \approx 1$ Hz, as in experiments discussed below, we find that the second term in Eq. (18) is smaller than the first term by a factor of approximately 10^{-12}. Therefore, considering that the experimental error of the damping constant γ in our experiments was in the 10 percent range (see Section 4), for the frequency ranges of interest in this paper the first order approximation is excellent,

$$\tilde{\gamma}_1 \approx \frac{2\gamma\omega_c}{\sqrt{\omega_1^2 - 4\gamma^2}} \approx 2\gamma\frac{\omega_c}{\omega_1}, \tag{19}$$

$$\tilde{\gamma}_\pm \approx \gamma\left(1 \pm \frac{\omega_c}{\sqrt{\omega_1^2 - 4\gamma^2}}\right) \approx \pm 2\gamma\frac{\omega_\pm}{\omega_1}. \tag{20}$$

It is equivalent to approximations used previously by König et al. [13]. Results obtained by them should therefore coincide with results obtained by our method of calculation.

Damping of the ion motion due to the presence of residual gas atoms dissipates part of the energy contained in the cyclotron and magnetron modes into kinetic energy of the residual gas. In most experimental setups we have $\omega_+ \gg \omega_-$, therefore with Eq. (20) we find in general a strong exponential decrease of the amplitude of the cyclotron mode and a slow exponential increase of the amplitude of the magnetron mode.

3.2. One-pulse quadrupole excitation

The measurement with the TOF-ICR method requires first the preparation of the ions in an almost pure magnetron orbit, secondly the resonant conversion of the magnetron motion into cyclotron motion by a pulse of rf-quadrupole radiation with a frequency $\nu_q = \omega_q/2\pi$ near to the cyclotron frequency ν_c and with duration τ, and finally a time-of-flight measurement of the ion energies. As discussed in greater detail below (see also Fig. 2), for rather weak damping the interconversion of the azimuthal motional modes resembles a Rabi type damped oscillation, but for stronger damping only the first maximum of the cyclotron mode survives. To obtain the maximum signal strength, the pulse duration τ must equal the conversion time τ_c, which is defined as the time at which the degree of conversion of the magnetron mode into the cyclotron mode reaches its first maximum. The cyclotron frequency ν_c, which is the main object of our interest, is deduced from a fit of the resonance curve to the TOF data as a function of the excitation frequency.

In Ref. [15] quadrupole excitation has been treated primarily from the quantum mechanical point of view as a process of conversion of single quanta of the cyclotron oscillator into quanta of the magnetron oscillator and vice versa. In this way the appropriate effective interaction Hamiltonian could be selected, which led to equations of motion for the annihilation operators of the oscillator quanta,

$$\dot{a}_+(\tau) = -i\omega_+ a_+(\tau) - ig\, e^{-i(\omega_q\tau+\chi_q)} a_-(\tau), \tag{21}$$

$$\dot{a}_-(\tau) = +i\omega_- a_-(\tau) - ig\, e^{+i(\omega_q\tau+\chi_q)} a_+(\tau), \tag{22}$$

and corresponding equations for creation operators of the quanta. Here ω_q and χ_q denote the angular frequency and phase of the applied quadrupole rf-pulse and g is a coupling parameter proportional to the amplitude of the rf-pulse. Classical quantities were then obtained as expectation values for coherent oscillator states, for example the complex oscillator amplitudes $\alpha_\pm(\tau)$ were obtained as expectation values of the annihilation operators $a_\pm(\tau)$ for cyclotron and magnetron quanta. Since the interaction with the quadrupolar field has been established in [15] it suffices for the present discussion to adopt the classical view point. Combining the Eqs. (14), (15) with the classical analogs of Eqs. (21), (22) our treatment of damped ion motion shall be based on the following Newtonian equations of motion

$$\dot{\alpha}_+(\tau) = -i\bar{\omega}_+ \alpha_+(\tau) - ig\, e^{-i(\omega_q\tau+\chi_q)} \alpha_-(\tau), \tag{23}$$

$$\dot{\alpha}_-(\tau) = +i\bar{\omega}_-^* \alpha_-(\tau) - ig\, e^{+i(\omega_q\tau+\chi_q)} \alpha_+(\tau). \tag{24}$$

These equations describe in the limit $g \to 0$ the ion motion in the ideal Penning trap with damping, Eqs. (16), (17) above, and in the limit $\gamma \to 0$ the quadrupole excitation in the undamped Penning trap, corresponding to Eqs. (21), (22). Either by explicit construction of the solution of the Eqs. (23), (24) or by the analytic continuation technique applied to Eqs. (21), (22) one finds the complex oscillator amplitudes that describe quadrupole excitation in the Penning trap with damping,[2]

$$\alpha_+(\tau) = \exp\left[-\frac{i}{2}(\tilde{\omega}_1 + \omega_q)\tau\right] \cdot \exp[-\gamma\tau] \times \left[\left(\cos\frac{\bar{\omega}_R\tau}{2} + i\frac{\delta + i\tilde{\gamma}_1}{\bar{\omega}_R}\sin\frac{\bar{\omega}_R\tau}{2}\right)\alpha_+(0) - i\frac{2g}{\bar{\omega}_R}\sin\frac{\bar{\omega}_R\tau}{2}e^{-i\chi_q}\alpha_-(0)\right], \tag{25}$$

$$\alpha_-(\tau) = \exp\left[-\frac{i}{2}(\tilde{\omega}_1 - \omega_q)\tau\right] \cdot \exp[-\gamma\tau] \times \left[-i\frac{2g}{\bar{\omega}_R}\sin\frac{\bar{\omega}_R\tau}{2}e^{i\chi_q}\alpha_+(0) + \left(\cos\frac{\bar{\omega}_R\tau}{2} - i\frac{\delta + i\tilde{\gamma}_1}{\bar{\omega}_R}\sin\frac{\bar{\omega}_R\tau}{2}\right)\alpha_-(0).\right] \tag{26}$$

The quantity $\delta = \omega_q - \omega_c$ denotes the detuning of the quadrupole rf-pulse from the cyclotron frequency. In the absence of damping the conversion process is controlled by the Rabi frequency $\omega_R = \sqrt{4g^2 + \delta^2}$. With damping the Rabi frequency becomes a complex quantity. Defining

$$\bar{\delta} = \delta + i\tilde{\gamma}_1, \tag{27}$$

[2] Note the occurrence of $\bar{\omega}_-^*$ instead of $\bar{\omega}_-$ in Eq. (24). This is required, because analytical continuation based on Eq. (5) relates to $\alpha_+(\tau)$ and $\alpha_-^*(\tau)$ (see Eqs. (16) and (17)), whereas the equations for quadrupole excitation relate to $\alpha_+(\tau)$ and $\alpha_-(\tau)$. The replacement of $\bar{\omega}_-$ with $\bar{\omega}_-^*$ in Eq. (24) is mathematically equivalent with the mutual exchange of 2γ and $\tilde{\gamma}_1$. Unfortunately, this point has escaped the attention of the author of [8] (M.K.), but the exchange $2\gamma \rightleftharpoons \tilde{\gamma}_1$ in the definitions of $\bar{\delta}$ and $\bar{\omega}_R$ and in Eqs. (48)–(56) of [8] corrects all results in Section 5 of [8]. Due to the large experimental uncertainty in the damping constant it is practically not possible to distinguish between 2γ and $\tilde{\gamma}_1$.

the construction of the solutions (25), (26) requires

$$\begin{aligned}\bar{\omega}_R &= \sqrt{4g^2+\bar{\delta}^2} = \sqrt{4g^2+\delta^2-\tilde{\gamma}_1^2+2i\delta\tilde{\gamma}_1} \\ &= \Re(\bar{\omega}_R)+i\Im(\bar{\omega}_R) = \tilde{\omega}_R - i\tilde{\gamma}_R.\end{aligned} \tag{28}$$

A successful experiment requires a quadrupolar amplitude strong enough to overcome the damping effects. We therefore assume $4g^2 > \tilde{\gamma}_1$. Denoting by $\omega_R = \sqrt{4g^2+\delta^2}$ the Rabi frequency without damping we then find for the real and imaginary parts of $\bar{\omega}_R$

$$\begin{aligned}\tilde{\omega}_R &= \Re(\bar{\omega}_R) \\ &= \frac{1}{\sqrt{2}}\sqrt{\sqrt{\left(\omega_R^2-\tilde{\gamma}_1^2\right)^2+4\tilde{\gamma}_1^2\delta^2}+\omega_R^2-\tilde{\gamma}_1^2},\end{aligned} \tag{29}$$

$$\begin{aligned}\tilde{\gamma}_R &= -\Im(\bar{\omega}_R) \\ &= \mp\frac{1}{\sqrt{2}}\sqrt{\sqrt{\left(\omega_R^2-\tilde{\gamma}_1^2\right)^2+4\tilde{\gamma}_1^2\delta^2}-(\omega_R^2-\tilde{\gamma}_1^2)},\end{aligned} \tag{30}$$

The sign of the square root in Eq. (29) has been chosen so that $\Re(\bar{\omega}_R) = \tilde{\omega}_R \geq 0$, and in the last equation the upper and lower signs hold for positive and negative δ, respectively. Note that at the exact resonance ($\delta = 0$) the square root on the right side of Eq. (30) vanishes for damping constants satisfying $4g^2 \geq \tilde{\gamma}_1^2$, so that we have $\tilde{\gamma}_R|_{\delta=0} = 0$. The case $4g^2 \leq \tilde{\gamma}_1^2$ requires an analogous discussion.

For later use we note

$$|\bar{\omega}_R|^2 = \sqrt{\left(\omega_R^2-\tilde{\gamma}_1^2\right)^2+4\tilde{\gamma}_1^2\delta^2}. \tag{31}$$

Let us discuss now the experimentally expected conversion lineshape, which describes the degree of conversion as a function of the detuning $\delta = \omega_q - \omega_c$ of the rf-frequency from the cyclotron frequency. In the quantum mechanical description without damping [15] one considers the numbers of quanta present in the cyclotron and magnetron modes at given time τ, $N_+(\tau)$ and $N_-(\tau)$, respectively. Quadrupolar excitation converts one type of quanta into the other, but leaves the sum invariant. In TOF-ICR mass spectrometry one prepares an initial state at time $\tau = 0$ in which only magnetron quanta are present, $N_-(0) = N_{tot}$ and $N_+(0) = 0$. Quadrupolar excitation of the cyclotron mode at frequencies near the cyclotron frequency ω_c is then described by the degree of conversion after a radiation pulse of duration τ, i.e., the relative number of cyclotron quanta then present in the system, $N_+(\tau)/N_{tot}$. In the quantum mechanical picture these numbers are given by the expectation values of the number operators $a_\pm^\dagger(\tau)a_\pm(\tau)$, which correspond in the classical picture to the absolute squares of the complex oscillator amplitudes $|\alpha_\pm(\tau)|^2 = m\omega_1/(2\hbar)\cdot R_\pm^2(\tau)$. These concepts are general and apply also when damping is present. We can therefore define the degree of conversion by a single pulse of radiation of duration τ and detuning δ by

$$F_1(\delta;\tau,g,\gamma) = \frac{|\alpha_+(\tau)|^2}{|\alpha_-(0)|^2} = \frac{R_+(\tau)^2}{R_-(0)^2}. \tag{32}$$

Inserting into this general definition our solution (25) of the equations of motion with damping we obtain

$$F_1(\delta;\tau,g,\gamma) = e^{-2\gamma\tau}\cdot\frac{4g^2}{|\bar{\omega}_R|^2}\left|\sin\left(\frac{\bar{\omega}_R\tau}{2}\right)\right|^2. \tag{33}$$

This result assumes pure magnetron motion as initial state ($\alpha_+(0) = 0, \alpha_-(0) \neq 0$) and is independent of the initial phases $\chi_\pm$ of the oscillators and χ_q of the quadrupolar rf-field. The observation of phase-dependent effects requires a sufficiently strong component of cyclotron motion in the starting configuration. With the substitutions (28)–(31) and the identities

$$\sin(\bar{\omega}_R\tau/2) = \sin(\tilde{\omega}_R\tau/2)\cdot\cosh(\tilde{\gamma}_R\tau/2) - i\cos(\tilde{\omega}_R\tau/2)\cdot\sinh(\tilde{\gamma}_R\tau/2), \tag{34}$$

$$\cos(\bar{\omega}_R\tau/2) = \cos(\tilde{\omega}_R\tau/2)\cdot\cosh(\tilde{\gamma}_R\tau/2) + i\sin(\tilde{\omega}_R\tau/2)\cdot\sinh(\tilde{\gamma}_R\tau/2), \tag{35}$$

and with $\cosh^2 x = 1+\sinh^2 x$ this becomes

$$\begin{aligned}F_1(\delta;\tau,g,\gamma) = {} & \frac{e^{-2\gamma\tau}\cdot 4g^2}{\sqrt{\left(4g^2+\delta^2-\tilde{\gamma}_1^2\right)^2+4\tilde{\gamma}_1^2\delta^2}} \\ & \cdot\left[\sin^2\frac{\tilde{\omega}_R\tau}{2}+\sinh^2\frac{\tilde{\gamma}_R\tau}{2}\right].\end{aligned} \tag{36}$$

To obtain the conversion line shape one has to plot this expression as a function of δ while keeping τ, g, γ constant. As in the undamped case $\gamma = 0$ the maximum of the central peak lies at $\delta = 0$, i.e., there is no line shift due to damping. The first term in the square bracket in Eq. (36) is present already in the undamped case $\gamma = 0$. With its zeroes at $\delta = 2g\sqrt{4n^2-1}$ ($n = 1, 2, 3, \ldots$) this term is mainly responsible for the excitation lineshape. In the presence of damping effects the positions of these zeroes are only marginally affected by the damping parameter γ. They are shifted to $\delta \approx 2g\sqrt{4n^2-1-\tilde{\gamma}_1^2/(16g^2)-3\tilde{\gamma}_1^4/(256g^4)}$, the central peak of the conversion lineshape is slightly broadened. Finally, the second term in the square brackets is not present in the undamped case $\gamma = 0$, but it grows in importance with increasing γ. As long as $\tilde{\gamma}_1^2 \leq 4g^2$ the second term vanishes at the resonance frequency, i.e., for $\delta = 0$ (see remarks after Eq. (30)), but for $\delta \neq 0$ it adds a positive contribution to the curve defined by the first term. It thus raises the excitation line shape, instead of zeroes we see minima at a non-zero positive level (for examples see the right hand side of Fig. 7).

It is of special interest to investigate the interconversion of modes at the exact resonance frequency ω_c. The relative number of cyclotron quanta present at time τ, i.e., $N_+(\tau)/N_{tot}$, is given by Eq. (36) as

$$\begin{aligned}P_+(\tau,g,\gamma) &= F_1(\delta;\tau,g,\gamma)|_{\delta=0} \\ &= \frac{e^{-2\gamma\tau}}{1-(\tilde{\gamma}_1/2g)^2}\cdot\sin^2\left(\sqrt{1-(\tilde{\gamma}_1/2g)^2}\cdot g\tau\right).\end{aligned} \tag{37}$$

Similarly, the relative number of magnetron quanta present at time τ, i.e., $N_-(\tau)/N_{tot}$, follows from Eq. (26) to be

$$\begin{aligned}P_-(\tau,g,\gamma) = {} & e^{-2\gamma\tau}\cdot\frac{1}{1-(\tilde{\gamma}_1/2g)^2} \\ & \cdot\left(\sqrt{1-(\tilde{\gamma}_1/2g)^2}\cdot\left(\cos\sqrt{1-(\tilde{\gamma}_1/2g)^2}\cdot g\tau\right)\right. \\ & \left.+(\tilde{\gamma}_1/2g)\cdot\sin\left(\sqrt{1-(\tilde{\gamma}_1/2g)^2}\cdot g\tau\right)\right)^2.\end{aligned} \tag{38}$$

These expressions describe, at the exact resonance frequency and starting with pure magnetron motion, the excitation of the cyclotron and magnetron modes as a function of the pulse duration of the quadrupole radiation. In the following we shall use the term excitation function to typify these functions.

For applications to TOF-ICR mass spectrometry the first conversion maximum is of special interest, because here we achieve the best possible degree of conversion of the magnetron into the cyclotron mode in the presence of damping. The time $\tau_c(g,\gamma)$ when this maximum is reached is defined as conversion time with damping. The extrema of the function $P_+(\tau)$ are deduced from the condition $(dP_+(\tau)/d\tau) = 0$, resulting in

$$\cot\left(\sqrt{1-\left(\tilde{\gamma}_1/(2g)\right)^2}\cdot g\tau - n\pi\right) = \frac{\gamma/g}{\sqrt{1-\left(\tilde{\gamma}_1/(2g)\right)^2}}, \tag{39}$$

with $n = 0$ for the first maximum and $n = 2, 4, 6, \ldots$ for subsequent maxima. Solving this condition for the time variable τ, using $n = 0$, we obtain the following expression for the 'conversion time with damping'

$$\tau_c(g, \gamma) = \frac{2}{\sqrt{4g^2 - \tilde{\gamma}_1^2}} \cdot \operatorname{arccot}\left(\frac{2\gamma}{\sqrt{4g^2 - \tilde{\gamma}_1^2}}\right). \quad (40)$$

For $\gamma = 0$ this is $\tau_c(g, 0) = \pi/(2g)$. The expression (40) is continuous at $g = \tilde{\gamma}_1/2$, but to avoid complex quantities we shall use for $g < \tilde{\gamma}_1/2$ the equivalent expression

$$\tau_c(g, \gamma) = \frac{2}{\sqrt{\tilde{\gamma}_1^2 - 4g^2}} \cdot \operatorname{arcoth}\left(\frac{2\gamma}{\sqrt{\tilde{\gamma}_1^2 - 4g^2}}\right). \quad (41)$$

We begin the discussion of the excitation functions by showing in Fig. 2 a 3D-plot of P_+ as function of the dimensionless time variable $\theta = \tau/\tau_c(g, 0) = (2g/\pi)\tau$ and of the ratio γ/g. For $\gamma/g = 0$ we have $P_+ = \sin((\pi/2)\theta)$, this pure sinus function represents the Rabi oscillation which is well known from treatments without damping effects. We have complete conversion into the cyclotron mode for $\theta = 1, 3, 5, \ldots$, and complete reconversion into the magnetron mode for $\theta = 2, 4, 6, \ldots$. For small values of γ/g the oscillation is damped, but still well visible. For stronger damping, say for $\gamma/g > 0.4$, only the first conversion peak is present, subsequent oscillations are suppressed by the exponential damping factor.

For a more detailed examination of the excitation functions P_+ and P_- we have plotted them in Fig. 3 as functions of the dimensionless variable θ and for $\gamma/g = 0.2$. The curves for $P_+(\theta, g, \gamma)$ (solid line) and for $P_+(\theta, g, \gamma)$ (long dashed line) both represent damped Rabi oscillations. Note that the first maximum of P_+ occurs earlier than in the undamped case, at a value $\theta < 1$, while the first minimum of P_- occurs later than in the undamped case, at a value $\theta > 1$. This is a consequence of the competition of the conversion process with the exponential damping. To understand this better consider in Fig. 3 the three intervals A, B, C. In the interval A ($0 < \theta < \tau_c(g, \gamma)/\tau_c(g, 0)$) the function $P_+(\theta)$ is increasing, the gain due to conversion is greater than the loss due to damping. Beyond the maximum, in interval B, the conversion of magnetron into modified cyclotron motion continues until no magnetron quanta are left, however the loss of modified cyclotron quanta due to damping is greater than the gain from conversion, thus the function $P_+(\theta)$ is now decreasing and the peak value is shifted toward lower θ. In interval C reconversion of modified cyclotron into magnetron motion occurs

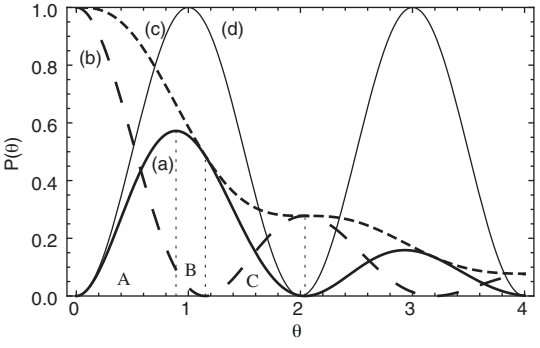

Fig. 3. Interplay of damping with the interconversion of oscillator quanta [Eqs. (37) and (38)]. The figure presents (a) $P_+(\theta)$ = relative number of cyclotron quanta (solid line), (b) $P_-(\theta)$ = relative number of magnetron quanta (long dashed line), and (c) $P_+(\theta) + P_-(\theta)$ = sum of all oscillator quanta (short dashed line), as functions of the dimensionless time variable $\theta = \tau/\tau_c(g, 0) = (2g/\pi)\tau$. The curves have been calculated for fixed values of quadrupole coupling $g = 3$ Hz and with a damping constant $\gamma = 0.6$ Hz ($\gamma/g = 0.2$). (d) For comparison the relative number of cyclotron quanta in the absence of damping is also shown (thin black line).

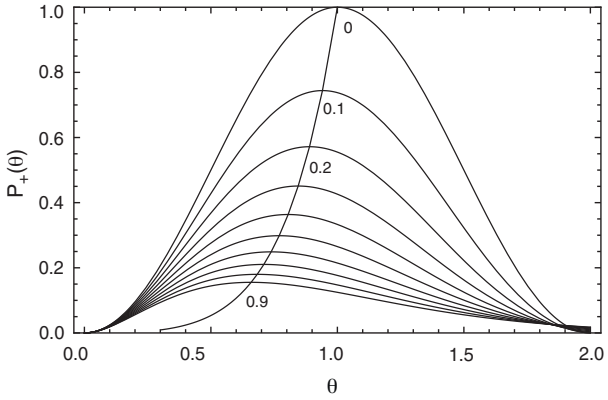

Fig. 4. The first maximum of the excitation function $P_+(\theta, \gamma/g)$, plotted for different values of γ/g (from top to bottom 0, 0.1, 0.2, . . ., 0.9). The line connecting the peak values has been calculated from Eq. (40).

until we have again pure magnetron motion. The distance between subsequent maxima of $P_+(\theta)$ is determined by the Rabi frequency $\omega_R = \sqrt{4g^2 - \tilde{\gamma}_1^2}$ (see Eq. (39)). Since the Rabi frequency is smaller than in the undamped case ($\omega_R = 2g$), the distance between subsequent maxima becomes somewhat larger. The decrease of the sum of the two excitation functions $P_+ + P_-$ (short dashed line) is not simply exponential, but follows a more complicated pattern which reflects the fact that the modified cyclotron mode suffers a fast decay with decay constant $\tilde{\gamma}_+ > 0$, while the magnetron mode slowly increases, $\tilde{\gamma}_- < 0$.

The fact that damping shifts the first conversion peak toward shorter conversion times as compared to the case without damping is expressed by $\tau_c(g, \gamma) < \tau_c(g, 0) = \pi/(2g)$. At the same time the maximum degree of conversion is lower than without damping. For strong damping this effect can be sizeable. To illustrate this effect we have plotted in Fig. 4 the first maximum for 10 different values $0 \le \gamma/g \le 0.9$. The line connecting the peak values has been calculated from Eq. (40).

The preceding discussion assumed the coupling parameter g, in more practical terms the amplitude of the quadrupole radiation pulse, to be fixed in the beginning, and the duration of the radiation pulse then to be chosen so as to produce the maximum degree of conversion into the cyclotron mode according to Eq. (40). For practical applications, however, as in the experiments described below, one rather prefers the reverse order: First to choose a pulse duration τ_{conv} according to the requirements of the specific experiment, and then to adjust the amplitude of the pulse so that a maximal conversion signal for a given value of γ is achieved. That implies that the coupling parameter g must be calculated numerically as a root of the equation $\tau_{conv} = \tau_c(g, \gamma)$, more explicitly

$$\tau_{conv} = \frac{2}{\sqrt{4g^2 - \tilde{\gamma}_1^2}} \cdot \operatorname{arccot}\left(\frac{2\gamma}{\sqrt{4g^2 - \tilde{\gamma}_1^2}}\right). \quad (42)$$

This procedure is illustrated in Fig. 5, which shows for a fixed value of γ the surface $F_1(\delta; \tau_{conv}, \gamma)$ plotted as function of $\delta' = \delta/2\pi$ and τ_{conv}, seen in a view showing high values of τ_{conv} in front and small values of τ_{conv} in the back. A cut through the figure at a given constant τ_{conv} represents the line profile for one-pulse quadrupole excitation with the amplitude (i.e., the coupling parameter g) chosen to give the maximum signal. Fig. 5 displays for increasing conversion time τ_{conv} the almost exactly exponentially decreasing height of the resonance signal, the shrinking of the width, and the disappearance of the fringe maxima except the central one.

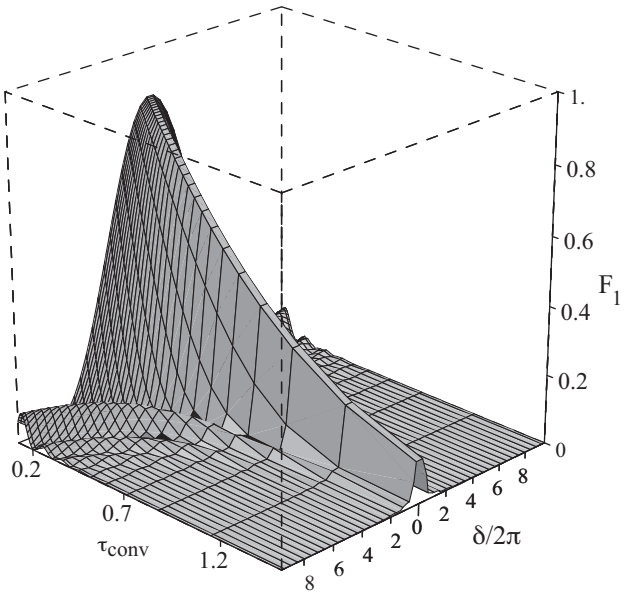

Fig. 5. Conversion of magnetron into cyclotron energy, $F_1(\delta; \tau_{conv}, \gamma)$, as a function of the frequency detuning $\delta' = \delta/(2\pi)$ and the excitation time τ_{conv}. Cuts through the surface at constant τ_{conv} are the one-pulse resonance signals with the quadrupole amplitude (g) chosen to give the maximum signal.

3.3. Ramsey excitation

For symmetric Ramsey excitation two pulses of rf-quadru-pole radiation with driving frequency $\omega_q \approx \omega_c$ and of equal duration τ_1 are applied, which are separated by a waiting interval of duration τ_0. The total excitation time is $\tau_{tot} = 2\tau_1 + \tau_0$. The observed line shape is described by a profile function

$$F_2(\delta; \tau_0, \tau_1, g, \gamma) = \frac{|\alpha_+(\tau_{tot})|^2}{|\alpha_-(0)|^2} = \frac{R_+(\tau_{tot})^2}{R_-(0)^2}. \quad (43)$$

The right hand side is evaluated by computing $\alpha_+(\tau_{tot})$ by means of Eqs. (25) and (26). The initial values $\alpha_\pm(0)$ of an ion trajectory are determined by the ion's initial position and initial velocity in the Penning trap, see Eqs. (103) and (104) in [15]. Let us assume $\alpha_+(0) = 0$ and $\alpha_-(0) = e^{i\chi_-}\sqrt{m\omega_1/(2\hbar)}R_-(0)$. Then there are three steps: starting from the initial values $\alpha_\pm(0)$ one calculates $\alpha_\pm(\tau_1)$ using the coupling parameter $g \neq 0$. The phase of the quadrupole field at time $t = \tau_1$ is $e^{i(\omega_q\tau_1+\chi_q)}$. With these results as initial data one calculates the changes during the waiting period τ_0, using a coupling parameter $g = 0$. During the waiting period there is no interconversion of the oscillator modes, the moduli $|\alpha_\pm(\tau)|$ remain constant, but the phases of the oscillator modes are changing. The results obtained for time $t = \tau_1 + \tau_0$ are used as initial data for the final step, in which we calculate the effect of the second radiation pulse. The result is

$$F_2(\delta; \tau_0, \tau_1, g, \gamma) = e^{-2\gamma(2\tau_1+\tau_0)} \cdot \frac{4g^2}{|\bar{\omega}_R|^2}\left|\cos\frac{\bar{\delta}\tau_0}{2}\sin(\bar{\omega}_R\tau_1) + \frac{\bar{\delta}}{\bar{\omega}_R}\sin\frac{\bar{\delta}\tau_0}{2}(\cos(\bar{\omega}_R\tau_1) - 1)\right|^2. \quad (44)$$

For the evaluation of the right hand side we have to use $\bar{\delta} = \delta + i\tilde{\gamma}_1$, Eqs. (28)–(31), the identities (34), (35) with $\tau = 2\tau_1$, and

$$\sin(\bar{\delta}\tau_0/2) = \sin(\delta\tau_0/2)\cdot\cosh(\tilde{\gamma}_1\tau_0/2) + i\cos(\delta\tau_0/2)\cdot\sinh(\tilde{\gamma}_1\tau_0/2), \quad (45)$$

$$\cos(\bar{\delta}\tau_0/2) = \cos(\delta\tau_0/2)\cdot\cosh(\tilde{\gamma}_1\tau_0/2) - i\sin(\delta\tau_0/2)\cdot\sinh(\tilde{\gamma}_1\tau_0/2). \quad (46)$$

The same results are obtained by applying the method of analytic continuation (with $\omega_R \to \bar{\omega}_R^*$) directly to Eq. (90) of [15].

Setting up the numerical evaluation of Eq. (44) requires some care, e.g., one must avoid numerical inaccuracies due to the evaluation of differences of almost equal large numbers.

4. Experimental results

Our experimental investigation of damping effects has focused on two important aspects of TOF-ICR mass spectrometry: (a) the degree of conversion of the magnetron into the cyclotron motional mode for continuous quadrupolar excitation at the exact cyclotron frequency. (b) The influence of damping on the line profiles of conventional one-pulse excitation and of two-pulse Ramsey excitation as a function of the damping constant γ.

4.1. Continuous excitation at the exact cyclotron frequency

The main topic of interest is the modification by damping effects of the Rabi-like oscillation pattern of the degree of conversion as

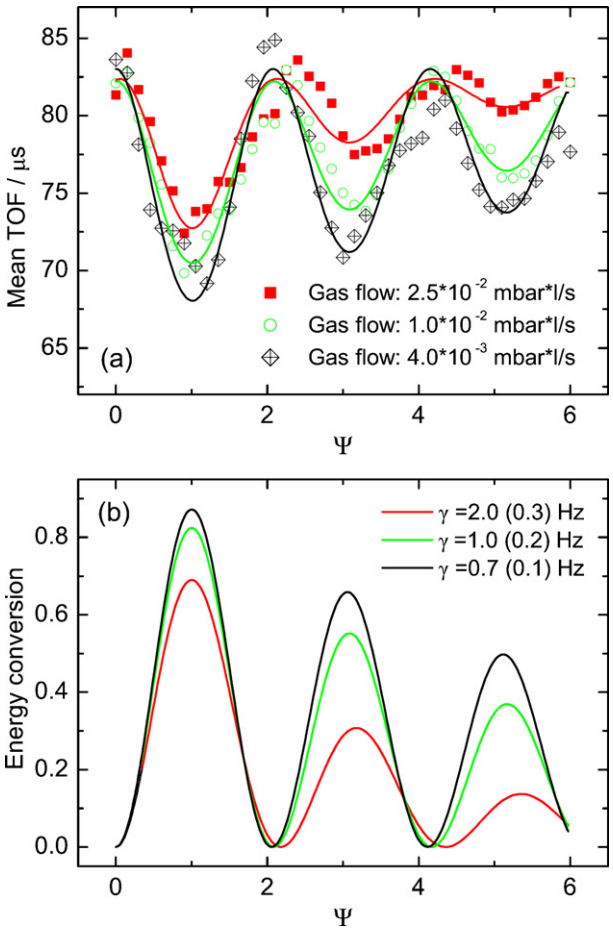

Fig. 6. (a) Mean time-of-flight results are displayed as functions of Ψ for different helium gas flow rates in the preparation trap of SHIPTRAP. The ion species used in these measurements was $^{133}Cs^+$. The lines are fits of the theoretical curves to the data. (b) Here, the calculated degree of conversion of magnetron into cyclotron energy at the exact resonance of the quadrupolar excitation, $F_1(\delta = 0; \tau, g, \gamma) = (R_+(\tau)/R_-(0))^2$ (Eq. (37)), as a function of time in units of the conversion time $\tau_c(g, \gamma)$ (Eq. (40)), i.e., time is plotted as the dimensionless variable $\Psi = \tau/\tau_c(g, \gamma)$. The damping coefficients γ are corresponding to those extracted from the experimental time-of-flight curves in (a) (color online).

described by Eq. (37), especially the exponential decrease of the height of the maxima with increasing excitation time and the shift of the positions of the maxima and minima (see Fig. 3).

The experiment described here has been performed at the SHIPTRAP facility. ^{133}Cs ions from the reference ion source were stored in the precision trap and prepared in a pure magnetron mode. To this end they were exposed to a background helium pressure which is responsible for the damping of the ion motion. This pressure is mainly due to the flow of helium buffer-gas from the preparation trap to the precision trap, although the gas flow is suppressed by a differential pumping barrier [26]. Since only differential pumping hampers the gas flow between the two traps, the gas flow rate to the preparation trap can be used to effectively control the pressure in the precision trap.

A series of measurements has been performed as follows. At constant background pressure quadrupolar rf-radiation at the cyclotron frequency ν_c is applied. The rf-amplitude is adjusted in such a way that a maximal conversion signal, and thus the strongest contrast in the time of flight of excited and non-excited ions, is obtained after an excitation time $\tau_c(g, \gamma) = \tau_{conv} = 100$ ms (Eq. (40)). Then for various excitation times τ between 0 and 600 ms the radial energy of the ions is probed via a time-of-flight measurement. The measurement is repeated several times with different values of the background pressure. Note that the background pressure in the environment of a Penning trap mass spectrometer is usually stable enough that the adjustment of the rf-amplitude has to be performed only once during a measurement period of a few days.

The observed damped Rabi oscillations, measured for three different gas flow rates, are shown in Fig. 6(a), where the mean time of flight is a function of $\Psi = \tau/\tau_c(g, \gamma)$. Each of the oscillation curves is generated by approximately 4000 ions. Fits of the theoretical line shape have been added to the data points and the damping coefficients γ have been extracted. The theoretical line shape of the time-of-flight curve is directly derived from a non-linear conversion of Eq. (37). For further details see [13]. A gas flow rate of 4×10^{-3} mbar l/s (diamonds), which is in the order of the normal flow rate during a mass measurement at SHIPTRAP, yields a damping coefficient of $\gamma = 0.7$ Hz (black line). Gas flow rates of 1×10^{-2} mbar l/s (open circles) and 2.5×10^{-2} mbar l/s (red squares) yield damping coefficients of $\gamma = 1.0$ Hz (green line) and $\gamma = 2.0$ Hz (red line), respectively. The extracted damping coefficients are used to calculate the corresponding energy conversion curves shown in Fig. 6(b). The exponential decrease of the maxima of the radial energy as time advances is apparent. The increase of the Rabi period $2\pi/\sqrt{4g^2 - \tilde{\gamma}_1^2}$ with increasing γ, here expressed in an occurrence of the maxima at larger $\Psi = \tau/\tau_c(g, \gamma)$ (see Fig. 6), is clearly observable and agrees with the expectations.

4.2. Conventional one-pulse excitation

Of greater interest for the application to mass measurements are the modifications of the resonance profiles by damping effects. The line profile is a direct consequence of the applied excitation pattern. For conventional one-pulse excitation the quadrupolar rf-field is applied with constant amplitude for a time interval τ_{conv}.

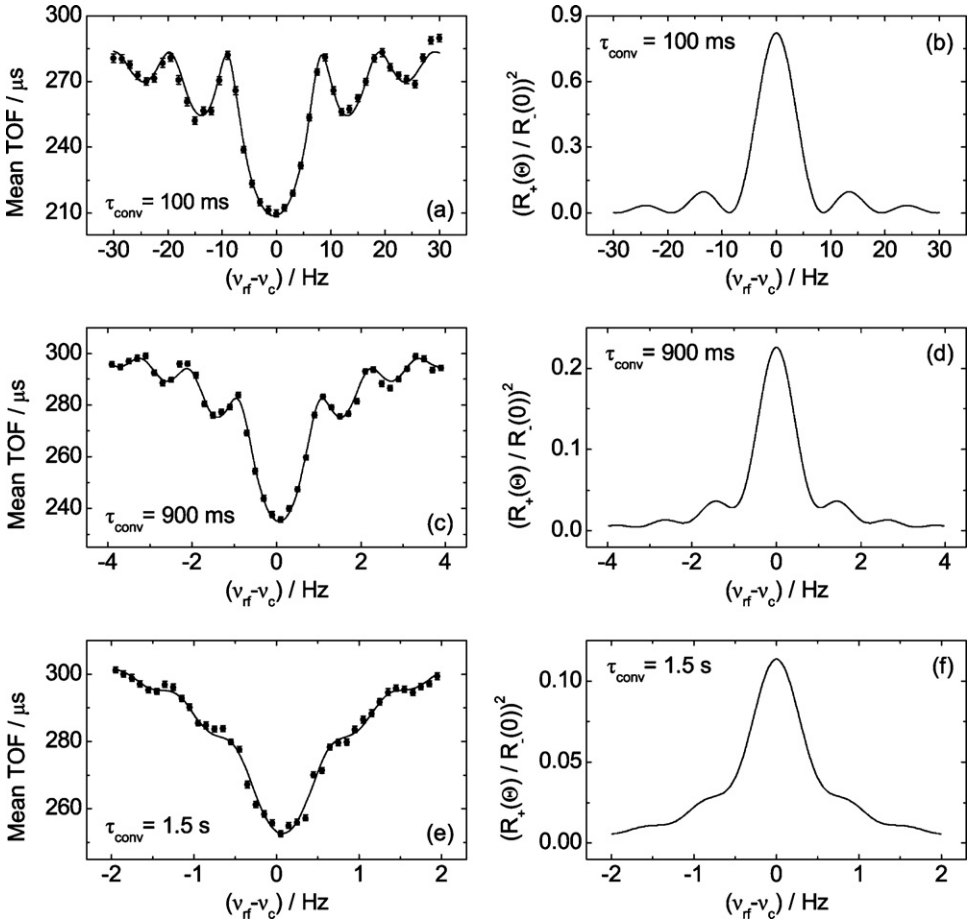

Fig. 7. Left: time-of-flight ion-cyclotron-resonance spectra measured at ISOLTRAP with ^{39}K ions. The excitation time is $\tau_{conv} = 100$ ms (a, b) in the first row, 900 ms (c, d) in the second row, and 1.5 s (e, f) in the third row, respectively. The solid lines are fits of the theoretical curves to the experimental data. Right: the degree of conversion from the initial magnetron mode into the cyclotron mode for a standard one-pulse excitation, $F_1(\delta; \tau_{conv}, g, \gamma) = (R_+(\tau_{conv})/R_-(0))^2$ for different excitation times τ_{conv}. The damping coefficient used for the calculations has been extracted from the corresponding resonance curves in the left column and is $\gamma = 1.0$ (0.1) Hz.

This situation has been analyzed theoretically in Section 3.2. Here we report on the corresponding experiments. TOF-ICR curves of ^{39}K ions as shown in Fig. 1 have been recorded at ISOLTRAP in the presence of an enhanced background pressure. The pumping power in the setup was reduced to increase the pressure from initially a few times 10^{-8} mbar to $1.1 \cdots 1.3 \times 10^{-6}$ mbar over a period of five days. Conventional TOF-ICR curves with various excitation times ranging from 100 ms up to 3 s with approximately 20,000 ions in each resonance have been recorded.

For a predetermined excitation time τ_{conv} the amplitude of the quadrupolar field is adjusted so that the conversion signal is maximal, in other words, the amplitude is adjusted so that τ_{conv} corresponds to the conversion time defined by Eq. (40), $\tau_{conv} = \tau_c(g, \gamma)$. The damping coefficient γ depends by Eq. (1) on the ion mass, ion

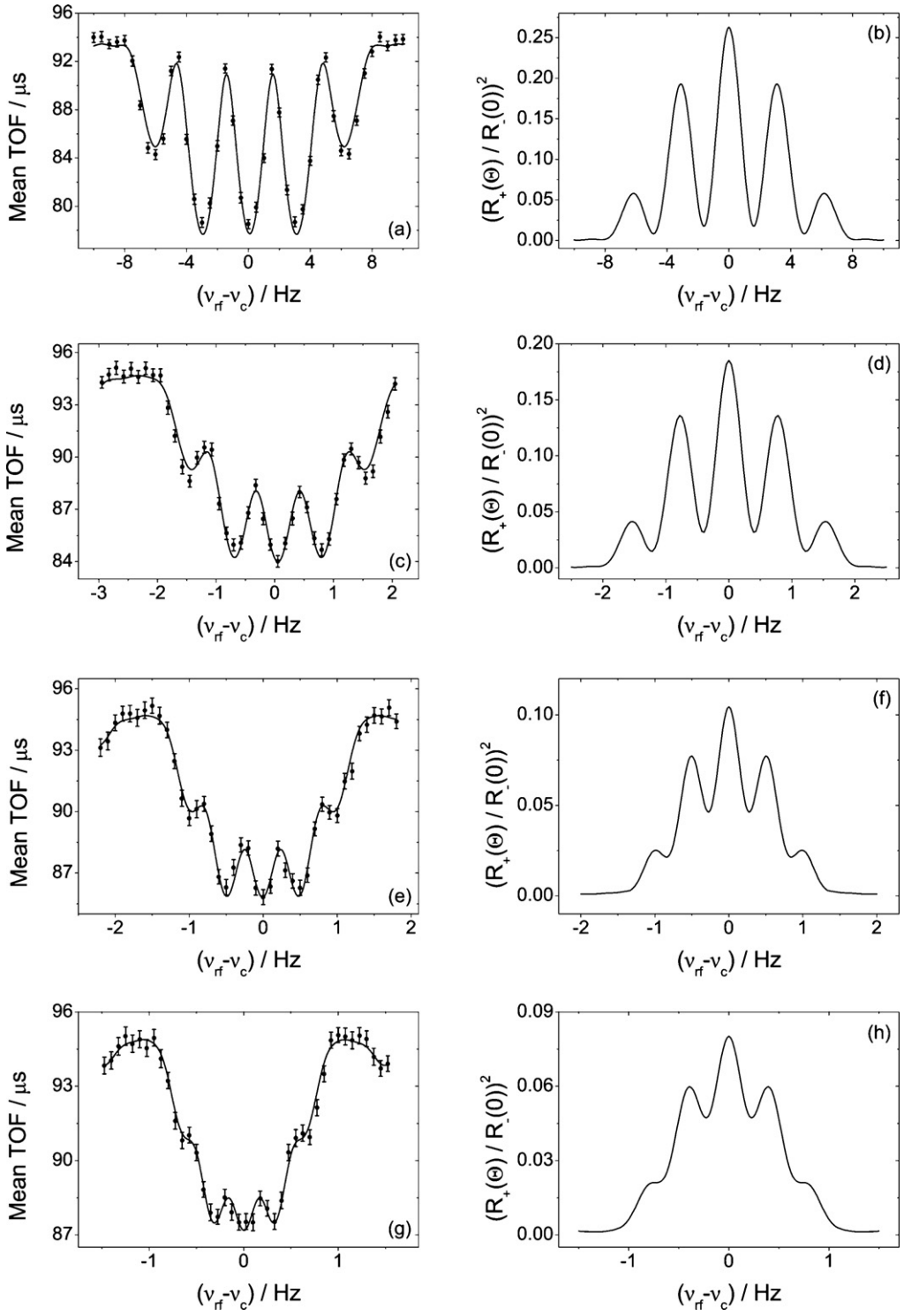

Fig. 8. Left time-of-flight ion-cyclotron-resonance spectra of $^{133}Cs^+$ taken at SHIPTRAP with fits of the theoretical curves (lines) to the data points. Excitation times: (a, b) $\tau_1 = 100$ ms, $\tau_0 = 200$ ms, (c, d) $\tau_1 = 200$ ms, $\tau_0 = 400$ ms, (e, f) $\tau_1 = 300$ ms, $\tau_0 = 600$ ms, (g, h) $\tau_1 = 900$ ms, $\tau_0 = 1800$ ms. Right: theoretical conversion line shapes $F_2(\bar{\delta}; \tau_0, \tau_1, g, \gamma) = (R_+(\tau_c(g, \gamma))/R_-(0))^2$ for Ramsey excitation pattern of two excitation periods τ_1 interrupted by a waiting time τ_0 [Eq. (44)]. The timings correspond the timings of the measured curves on the left side.

mobility, buffer-gas species, buffer-gas temperature and buffer-gas pressure. For ^{39}K ions moving at room temperature in a helium buffer-gas of pressure 1.1×10^{-6} mbar and with an ion mobility $K_0 \approx 21.5$ [cm^2/V s] (see [34]) one estimates $\gamma \approx 0.63$ Hz (see also Eq. (57) in [8]). For the temperature dependence of K_0 see [35]. With this value of γ the equation $\tau_{conv} = \tau_c(g, \gamma)$ can now be solved for the coupling parameter g, using Eq. (40). Now all information needed for the calculation of theoretical conversion profiles from Eq. (36) is at hand. After transformation into TOF-profiles these are fitted to the experimental TOF-curves.

Three examples of such curves with $\tau_{conv} = 100$ ms, 900 ms, and 1.5 s excitation time are shown in the left column of Fig. 7. The right column shows the corresponding theoretical energy conversion profiles for a damping constant $\gamma \approx 1$. The coupling parameters g for the three curves are calculated from Eq. (40) to be $g \approx 15.08$ Hz, 1.17 Hz, 0.515 Hz, respectively.

The modification due to damping of the shape of the conversion profile is governed, according to Eq. (36), by the dimensionless ratio γ/g. For our three curves we find the values $\gamma/g = 0.066$ (weak damping), 0.856 (medium strong damping), and 1.94 (very strong damping), respectively. Furthermore, all data have been evaluated twice: first, using the equations of motion found in König et al. [13], up to now used in the fitting routine. Second, the equations described in the theory section of this article have been used. No difference in the extracted resonance frequency and its uncertainty has been found for all measured curves, which span the pressure regime of a Penning trap applied for precision mass measurements.

4.3. Ramsey-type two-pulse excitation

The theoretical prediction for the line shape of symmetric two-pulse Ramsey excitation including damping effects, Eq. (44), has been tested at the SHIPTRAP facility using ^{133}Cs ions. Excitation schemes of two excitation periods τ_1 interrupted by a waiting time τ_0 have been applied to measure TOF resonances with relatively high background pressure corresponding to a damping coefficient $\gamma = 0.7$ Hz. The conversion times $\tau_c(g, \gamma) = 2\tau_1$ are obtained by a suitable adjustment of the amplitude of the quadrupole rf-field, which is equivalent to a suitable choice of the coupling parameter g. According to Eq. (40) the chosen conversion times $\tau_c(g, \gamma) = 200$, 400, 600, and 1800 ms (see Fig. 8) together with $\gamma = 0.7$ Hz imply $g \approx 7.41$, 3.49, 2.15, and 0.49 Hz, and thus ratios $\gamma/g \approx 0.09$, 0.20, 0.33, and 1.43. These ratios control the shape of the conversion profiles. Measured TOF profiles are shown in Fig. 8 (left column) and compared to the corresponding theoretical conversion profiles calculated from Eq. (44) (Fig. 8 (right column)). We conclude that the theoretical treatment presented in Section 3 describes the experimental data in a correct way.

5. Conclusion

The resonant conversion of magnetron motion into cyclotron motion by application of a quadrupolar rf-field with a frequency at the cyclotron frequency is a process of prime importance for mass spectrometry with Penning traps. In this paper we have investigated theoretically and experimentally how this process is influenced by damping due to the inevitable presence of neutral gas in the Penning trap. The theoretical considerations were based on the assumption that the damping force is linear in the velocity. This assumption seems reasonable given the excellent agreement with the experimental data. Using the recently developed method of analytical continuation with respect to the cyclotron frequency [8] we were able to present for the first time closed analytical expressions describing the conversion line shape for conventional one-pulse excitation and for symmetric two-pulse or Ramsey excitation in the presence of damping. Choosing the rf-amplitude so as to produce a maximal conversion signal for a given excitation time τ_{conv} we find that the signal decreases exponentially due to damping with increasing excitation time, while the shape of the resonance depends on the ratio γ/g of the damping constant γ and the coupling parameter g, loosing structure as this ratio varies from 0 to 1 and beyond. The theoretical results have been checked against experimental data taken at the ISOLTRAP and SHIPTRAP facilities with various ion species and under a variety of pressure conditions. No significant deviations from the theoretical description have been found. Thus the results can be used with confidence in applications of Penning trap mass spectrometry.

Acknowledgements

This work was supported by the German BMBF under contracts 06MZ215, 06GF186I, and 06GF9102, by the EU within the 6th Framework through RII3-EURONS (contract no. 506065) and Marie Curie Fellowship MEIF-CT-2006-042114, by the Helmholtz association of national research centers (HGF) under contract VH-NG-037 and by the Max-Planck Society.

References

[1] K. Blaum, Phys. Rep. 425 (2006) 1.
[2] L. Schweikhard, G. Bollen (Eds.), Int. J. Mass Spectrom. 251 (2006) (special issue).
[3] K. Blaum, Yu.N. Novikov, G. Werth, Contemp. Phys. 51 (2) (2010) 149.
[4] C. Rauth, D. Ackermann, K. Blaum, M. Block, A. Chaudhuri, Z. Di, S. Eliseev, R. Ferrer, D. Habs, F. Herfurth, F.P. Heßberger, S. Hofmann, H.-J. Kluge, G. Maero, A. Martin, G. Marx, M. Mukherjee, J.B. Neumayr, W.R. Plaß, S. Rahaman, D. Rodrıguez, C. Scheidenberger, L. Schweikhard, P.G. Thirolf, G. Vorobjev, C. Weber, Phys. Rev. Lett 100 (2008) 012501.
[5] M. Block, D. Ackermann, K. Blaum, C. Droese, M. Dworschak, S. Eliseev, T. Fleckenstein, E. Haettner, F. Herfurth, F.P. Heßberger, S. Hofmann, J. Ketelaer, J. Ketter, H.-J. Kluge, G. Marx, M. Mazzocco, Yu.N. Novikov, W.R. Plaß, A. Popeko, S. Rahaman, D. Rodriguez, C. Scheidenberger, L. Schweikhard, P.G. Thirolf, G.K. Vorobyev, C. Weber, Nature 463 (2010) 785.
[6] D. Neidherr, G. Audi, D. Beck, K. Blaum, Ch. Böhm, M. Breitenfeldt, R.B. Cakirli, R.F. Casten, S. George, F. Herfurth, A. Herlert, A. Kellerbauer, M. Kowalska, D. Lunney, E. Minaya-Ramirez, S. Naimi, E. Noah, L. Penescu, M. Rosenbusch, S. Schwarz, L. Schweikhard, T. Stora, Phys. Rev. Lett. 102 (2009) 112501.
[7] L.S. Brown, G. Gabrielse, Rev. Mod. Phys. 58 (1986) 233.
[8] M. Kretzschmar, Eur. Phys. J. D 48 (3) (2008) 313.
[9] P.K. Ghosh:, Ion Traps, Clarendon Press, Oxford, 1995.
[10] F.G. Major, V.N. Gheorghe, G. Werth, Charged Particle Traps, Physics and Techniques of Charged Particle Field Confinement (Springer Series on Atomic, Optical, and Plasma Physics, vol. 37), Springer-Verlag, Berlin, 2005.
[11] G. Savard, St. Becker, G. Bollen, H.-J. Kluge, R.B. Moore, Th. Otto, L. Schweikhard, H. Stolzenberg, U. Wiess, Phys. Lett. A 158 (1991) 247.
[12] G. Gräff, H. Kalinowsky, J. Traut, Z. Phys. A 297 (1980) 35.
[13] M. König, G. Bollen, H.-J. Kluge, T. Otto, J. Szerypo, Int. J. Mass Spectrom. Ion Process 142 (1995) 95.
[14] G. Bollen, H.-J. Kluge, T. Otto, G. Savard, H. Stolzenberg, Nucl. Instrum. Meth. B 70 (1992) 490.
[15] M. Kretzschmar, Int. J. Mass. Spectrom. 264 (2007) 122.
[16] S. George, K. Blaum, F. Herfurth, A. Herlert, M. Kretzschmar, S. Nagy, S. Schwarz, L. Schweikhard, C. Yazidjian, Int. J. Mass Spectrom. 264 (2007) 110.
[17] S. George, S. Baruah, B. Blank, K. Blaum, M. Breitenfeldt, U. Hager, F. Herfurth, A. Herlert, A. Kellerbauer, H.-J. Kluge, M. Kretzschmar, D. Lunney, R. Savreux, S. Schwarz, L. Schweikhard, C. Yazidjian, Phys. Rev. Lett. 98 (2007) 162501.
[18] T. Eronen, V.-V. Elomaa, U. Hager, J. Hakala, A. Jokinen, A. Kankainen, S. Rahaman, J. Rissanen, C. Weber, J. Äystö, Nucl. Instrum. Meth. B 266 (2007) 4527.
[19] S. George, G. Audi, B. Blank, K. Blaum, M. Breitenfeldt, U. Hager, F. Herfurth, A. Herlert, A. Kellerbauer, H.-J. Kluge, M. Kretzschmar, D. Lunney, R. Savreux, S. Schwarz, L. Schweikhard, C. Yazidjian, Europhys. Lett. 50005 (2008) 1.
[20] T. Eronen, V.-V. Elomaa, U. Hager, J. Hakala, J.C. Hardy, A. Jokinen, A. Kankainen, I.D. Moore, H. Penttilä, S. Rahaman, S. Rinta-Antila, J. Rissanen, A. Saastamoinen, T. Sonoda1, C. Weber, J. Äystö, Phys. Rev. Lett. 100 (2008) 132502.
[21] N.D. Scielzo, S. Caldwell, G. Savard, J.A. Clark, C.M. Deibel, J. Fallis, S. Gulick, D. Lascar, A.F. Levand, G. Li, J. Mintz, E.B. Norman, K.S. Sharma, M. Sternberg, T. Sun, J. Van Schelt, Phys. Rev. C 80 (2009) 025501.
[22] M. Mukherjee, D. Beck, K. Blaum, G. Bollen, J. Dilling, S. George, F. Herfurth, A. Herlert, A. Kellerbauer, H.-J. Kluge, S. Schwarz, L. Schweikhard, C. Yazidjian, Eur. Phys. J. A 35 (2008) 1.
[23] M. Block, D. Ackermann, D. Beck, K. Blaum, M. Breitenfeldt, A. Chauduri, A. Doemer, S. Eliseev, D. Habs, S. Heinz, F. Herfurth, F.P. Heßberger, S. Hofmann, H. Geissel, H.-J. Kluge, V. Kolhinen, G. Marx, J.B. Neumayr, M. Mukherjee, M. Petrick, W. Plass, W. Quint, S. Rahaman, C. Rauth, D. Rodriguez, C. Scheidenberger,

L. Schweikhard, M. Suhonen, P.G. Thirolf, Z. Wang, C. Weber, the SHIPTRAP Collaboration, Eur. Phys. J. A 25 (S01) (2005) 49.
[24] F. Herfurth, J. Dilling, A. Kellerbauer, G. Bollen, S. Henry, H.-J. Kluge, E. Lamour, D. Lunney, R.B. Moore, C. Scheidenberger, S. Schwarz, G. Sikler, J. Szerypo, Nucl. Instrum. Meth. A 469 (2001) 254.
[25] C. Yazidjian, K. Blaum, R. Ferrer, F. Herfurth, A. Herlert, L. Schweikhard, Hyperfine Int 173 (2006) 181.
[26] D. Neidherr, K. Blaum, M. Block, R. Ferrer, F. Herfurth, J. Ketelaer, Sz. Nagy, C. Weber, Nucl. Instrum. Meth. Phys. Res. B 266 (2008) 4556.
[27] K. Blaum, G. Bollen, F. Herfurth, A. Kellerbauer, H.-J. Kluge, M. Kuckein, S. Heinz, P. Schmidt, L. Schweikhard, J. Phys. B: At. Mol. Opt. Phys 36 (2003) 921.
[28] G. Bollen, R.B. Moore, G. Savard, H. Stolzenberg, J. Appl. Phys. 68 (1990) 4355.
[29] G. Gabrielse, Int. J. Mass. Spectrom. 279 (2009) 107.
[30] L. Schweikhard, A.G. Marshall, J. Am. Soc. Mass Spectrom. 4 (1993) 433.
[31] E.A. Mason, E.W. McDaniel:, Transport Properties of Ions in Gases, John Wiley and Sons, New York, 1988.
[32] R.B. Moore: Buffer Gas Cooling of Ion Beams, January 2002. www.physics.mcgill.ca/~moore/Notes/Beam Cooling.pdf. See also Abstract CERN - EP/2000-048.
[33] S. Schwarz, Simulations for ion traps – buffer gas cooling in trapped charged particles and fundamental interactions, in: K. Blaum, F. Herfurth (Eds.), Lecture Notes in Physics, vol. 749, Springer-Verlag, Berlin, Heidelberg, 2008.
[34] H.R. Skullerud, M.T. Elford, I. Roeggen, J. Phys. B: At. Mol. Opt. Phys. 29 (1996) 1925.
[35] M. Bouledroua, F. Bouchelaghem, 19th Europhysics Conference on the Atomic and Molecular Physics of Ionized Gases, Granada (Spain), 15–19 July 2008, www.escampig2008.csic.es/PosterSessions/5.pdf.